Kwon et al. *Zool. Res.* 2025, 46(1): 165−176
https://doi.org/10.24272/j.issn.2095-8137.2024.277
https://cstr.cn/32248.14.zr.2024.277

ZR | Zoological Research

Article Open Access

Deciphering the toxic effects of polystyrene nanoparticles on erythropoiesis at single-cell resolution

Eun Jung Kwon[1,#], Hyeon Mi Sung[2,3,#], Hansong Lee[1], Soyul Ahn[2,3], Yejin Kim[2,3], Chae Rin Lee[2,3], Kihun Kim[4,5], Kyungjae Myung[6,7], Won Kyu Kim[8,9,10], Dokyoung Kim[11,12,13,14,15,16,17,18], Sanghwa Jeong[19,*], Chang-Kyu Oh[2,20,*], Yun Hak Kim[4,5,*]

[1] *Medical Research Institute*, *Pusan National University*, *Yangsan*, *Gyeongsangnam-do* 50612, *Republic of Korea*
[2] *Institute for Future Earth*, *Pusan National University*, *Busan* 46241, *Republic of Korea*
[3] *Department of Convergence Medical Sciences*, *School of Medicine*, *Pusan National University*, *Yangsan*, *Gyeongsangnam-do* 50612, *Republic of Korea*
[4] *Department of Biomedical Informatics*, *School of Medicine*, *Pusan National University*, *Yangsan*, *Gyeongsangnam-do* 50612, *Republic of Korea*
[5] *Department of Anatomy*, *School of Medicine*, *Pusan National University*, *Yangsan*, *Gyeongsangnam-do* 50612, *Republic of Korea*
[6] *Center for Genomic Integrity*, *Institute for Basic Science*, *Ulsan* 689-798, *Republic of Korea*
[7] *Department of Biomedical Engineering*, *College of Information-Bio Convergence Engineering*, *Ulsan National Institute of Science and Technology*, *Ulsan* 44919, *Republic of Korea*
[8] *Natural Product Research Center*, *Korea Institute of Science and Technology (KIST)*, *Gangneung*, *Gangwon-do* 25451, *Republic of Korea*
[9] *Department of Convergence Medicine*, *Yonsei University Wonju College of Medicine*, *Wonju*, *Gangwon-do* 26426, *Republic of Korea*
[10] *Natural Product Applied Science*, *KIST School*, *University of Science and Technology (UST)*, *Gangneung*, *Gangwon-do* 25451, *Republic of Korea*
[11] *Department of Biomedical Science*, *Graduate School*, *Kyung Hee University*, *Seoul* 02447, *Republic of Korea*
[12] *Department of Anatomy and Neurobiology*, *College of Medicine*, *Kyung Hee University*, *Seoul* 02447, *Republic of Korea*
[13] *Department of Precision Medicine*, *Graduate School*, *Kyung Hee University*, *Seoul* 02447, *Republic of Korea*
[14] *Center for Converging Humanities*, *Kyung Hee University*, *Seoul* 02447, *Republic of Korea*
[15] *KHU-KIST Department of Converging Science and Technology*, *Kyung Hee University*, *Seoul* 02447, *Republic of Korea*
[16] *UC San Diego Materials Research Science and Engineering Center*, 9500 *Gilman Drive*, *La Jolla*, *California* 92093, *USA*
[17] *Medical Research Center for Bioreaction to Reactive Oxygen Species and Biomedical Science Institute*, *Core Research Institute (CRI)*, *Kyung Hee University*, *Seoul* 02447, *Republic of Korea*
[18] *Center for Brain Technology*, *Brain Science Institute*, *Korea Institute of Science and Technology (KIST)*, *Seoul* 02792, *Republic of Korea*
[19] *School of Biomedical Convergence Engineering*, *Pusan National University*, *Yangsan*, *Gyeongsangnam-do* 50612, *Republic of Korea*
[20] *Department of Biochemistry*, *School of Medicine*, *Pusan National University*, *Yangsan*, *Gyeongsangnam-do* 50612, *Republic of Korea*

ABSTRACT

Polystyrene nanoparticles pose significant toxicological risks to aquatic ecosystems, yet their impact on zebrafish (*Danio rerio*) embryonic development, particularly erythropoiesis, remains underexplored. This study used single-cell RNA sequencing to comprehensively evaluate the effects of polystyrene nanoparticle exposure on erythropoiesis in zebrafish embryos. *In vivo* validation experiments corroborated the transcriptomic findings, revealing that polystyrene nanoparticle exposure disrupted erythrocyte differentiation, as evidenced by the decrease in mature erythrocytes and concomitant increase in immature erythrocytes. Additionally, impaired heme synthesis further contributed to the diminished erythrocyte population.

Received: 27 August 2024; Accepted: 22 November 2024; Online: 23 November 2024

Foundation items: This work was supported by the Institute for Basic Science (IBS-R022-D1), Global Learning & Academic Research Institution for Master's/PhD students and Post-Doc Program of the National Research Foundation of Korea Grant funded by the Ministry of Education (RS-2023-00301938), and National Research Foundation of Korea Grant funded by the Korean government (RS-2024-00406152, MSIT). Additional financial support was provided by the 2024 Post-Doc Development Program of Pusan National University, Korea Medical Institute, and KREONET

[#]Authors contributed equally to this work

*Corresponding authors, E-mail: sanghwa.jeong@pusan.ac.kr; ck1988@pusan.ac.kr; yunhak10510@pusan.ac.kr

These findings underscore the toxic effects of polystyrene nanoparticles on hematopoietic processes, highlighting their potential to compromise organismal health in aquatic environments.

Keywords: Polystyrene nanoparticles; Zebrafish embryos; Single-cell RNA sequencing; Erythropoiesis

INTRODUCTION

Plastics, known for their versatility, long lifespan, cost-effectiveness, and ability to replace heavier substances, such as metals and glass, have become indispensable in modern industries and contemporary life (Andrady & Neal, 2009). Common plastics include polyethylene, polyethylene terephthalate, polypropylene, polyvinyl chloride, and polystyrene (Andrady, 2011). Among these, polyethylene and polypropylene are extensively used in the production of disposable bags, bottle caps, and packaging materials, contributing significantly to marine plastic pollution (Schwarz et al., 2019; Thushari & Senevirathna, 2020). Polystyrene, valued for its relatively low cost and lightweight nature, is widely used in disposable tableware and toys. However, its aromatic ring structure renders it more toxic than polyethylene or polyethylene terephthalate, amplifying its potential ecological impact (Alimi et al., 2022).

In the natural environment, most plastics degrade gradually under the influence of sunlight, wind, and wave action, lacking microbial decomposition (Ekvall et al., 2019; Kik et al., 2020). This gradual degradation generates microplastics —particles smaller than 5 mm —which can bypass sewage treatment plants and accumulate in aquatic ecosystems (Law & Thompson, 2014). Microplastics are generally classified as either primary or secondary. Primary microplastics are intentionally manufactured as small particles, commonly incorporated into products such as cosmetics and detergents, or directly released into the marine environment (Cole et al., 2013; Wang et al., 2019). In contrast, secondary microplastics originate from the breakdown of larger plastic items through natural processes (Duis & Coors, 2016; Ogonowski et al., 2016). Both forms pose serious ecological threats, adversely affecting aquatic ecosystems and marine life, as well as contributing to water pollution. Recognizing these impacts, extensive research has been conducted to understand the environmental and biological consequences of microplastics in aquatic environments (Ryan et al., 2009).

In addition to microplastics, nanoplastics, which range from 1 nm to 1 μm in size (Jambeck et al., 2015), have garnered increasing attention due to their profound impact on aquatic ecosystems and organismal health. Notably, nanoplastics can infiltrate biological systems with great efficiency, accumulating in aquatic species such as fish, crustaceans, and shellfish. These particles have been implicated in cellular damage, growth inhibition, and ecosystem disruption (Timilsina et al., 2023). Studies have indicated that nanoparticle size plays a critical role in their absorption and distribution within tissues, with smaller particles exhibiting enhanced bioavailability and organ penetration (Wang et al., 2023). For instance, in Nile tilapia (*Oreochromis niloticus*), 0.1 μm polystyrene nanoparticles accumulate in the gills at levels 3.4-fold higher than those of 0.5 μm polystyrene nanoparticles, with approximately 0.8 μg per gram detected in the gills (Wang et al., 2023). Similarly, smaller particles have been shown to intensify neutrophil aggregation and macrophage apoptosis in the abdomen of zebrafish (*Danio rerio*) larvae, leading to significant hepatic inflammation (Cheng et al., 2022). The nanoscale size of these plastics allows them to easily penetrate cellular membranes, thereby disrupting growth, development, and metabolic processes in exposed organisms (Pedersen et al., 2020; Shen et al., 2019). The implications of nanoplastics extend to critical physiological systems. Studies have demonstrated their ability to pass through the blood-brain barrier, accumulating in brain tissue and potentially impairing brain function (Sökmen et al., 2020). Additionally, polystyrene nanoplastics have been shown to alter immune and secretory cell populations in the intestinal tissue of zebrafish (Gu et al., 2020), further highlighting their systemic effects.

The molecular mechanisms through which microplastics and nanoplastics exert their toxic effects on aquatic life remain unclear, despite extensive research into their impacts at cellular and tissue levels. Notably, while the influence of polystyrene nanoparticles on immune cells such as neutrophils and macrophages has been documented (Jiang et al., 2024; Zhu et al., 2022), their potential effects on erythropoiesis remain largely unexplored. Given that polystyrene nanoparticles are likely to interact with red blood cells (RBCs) during circulation, these cells may also be vulnerable to polystyrene-induced toxicity. However, research on the direct effects of these particles on RBCs, either *in vitro* or *in vivo*, is scarce.

In the current study, we hypothesized that exposure to polystyrene nanoparticles would negatively impact erythropoiesis in zebrafish embryos. To ensure precise concentration control and eliminate inaccuracies caused by nanoparticle penetration of chorion pores prior to 72 h post-fertilization (hpf), fully hatched zebrafish embryos were exposed to 20 nm polystyrene nanoparticles (PS20 nm) at 72 hpf. The exposure concentrations, ranging from 0.1 to 10 μg/mL, were selected to ensure adequate exposure and reflect levels found in natural water and marine environments (Wang et al., 2023). To rigorously test this hypothesis, both *in silico* and *in vivo* experiments were conducted. These complementary methodologies not only provided robust validation of the results but also aligned with findings from existing studies.

MATERIALS AND METHODS

Characterization of polystyrene nanoparticles

The hydrodynamic (HD) size of the polystyrene nanoparticles was determined using dynamic light scattering (DLS) with a Zetasizer Nano ZSP (Malvern PANalytical, UK). Measurements were conducted at 20°C in 1×phosphate-buffered saline (PBS) at pH 7.4, employing a non-invasive back-scattering mode at an angle of 173° under 633 nm excitation. High-resolution transmission electron microscopy (HR-TEM) images were obtained using a JEM-2100 instrument (JEOL, Japan). For HR-TEM sample preparation, a suspension of nanoparticles in water was dropped onto a standard TEM grid and allowed to dry under ambient conditions. Fourier transform infrared spectroscopy (FTIR) analysis was used to investigate the chemical structure of the nanoparticles. FTIR spectra were collected using an iS50 spectrometer (Thermo Fisher Scientific, USA) at a wavelength range of 4 000–400 cm^{-1}, with a standard KBr beam splitter in transmittance mode. Sample preparation involved repeated

filtration of the microbead dispersion using a 30 kDa molecular weight cutoff (MWCO) centrifugal filter to remove residual surfactants and salts. The filtered nanoparticles were suspended in deionized water, vacuum-dried, and mixed with KBr powder.

Zebrafish and embryo maintenance and chemical treatment

Wild-type zebrafish and *gata1:*DsRed transgenic zebrafish (provided by IBS, CGI, South Korea) were maintained in a fully automated circulation aquarium system (Techniplast, Maggio, Italy) at 28.5°C under a 14 h light/10 h dark cycle (pH: 7.0, electrical conductivity: 1 000 μS/cm). All procedures followed the guidelines of the Institutional Animal Care and Use Committee (IACUC) from Pusan National University (PNU-2023-0359). Zebrafish embryos were collected at 0.5 hpf and incubated at 28±1°C with E3 solution (14.61 g NaCl, 0.63 g KCl, 1.83 g $CaCl_2{\cdot}2H_2O$, and 1.99 g $MgSO_4$ in 1 L of deionized water). Polystyrene nanoparticles (Sigma-Aldrich, USA) were diluted in the E3 solution for exposure studies, with treatments applied daily from 72 hpf.

Confocal imaging of nanoparticle accumulation

To evaluate the biodistribution of polystyrene nanoparticles in zebrafish embryos, polystyrene nanoparticles at concentrations of 0.1–10 μg/mL were prepared. Embryos were anesthetized with 2 g of tricaine (Sigma-Aldrich, USA) dissolved in 1 L of E-pure water and mounted in 3% methylcellulose on a glass-bottomed culture dish. Samples were observed and imaged using a confocal microscope (LSM880; Carl Zeiss, Germany).

Sampling for single-cell RNA sequencing

Zebrafish embryos were sacrificed at 120 hpf using 2 g of tricaine (Sigma-Aldrich, USA) dissolved in 1 L of E-pure water. Sacrificed embryos were incubated with 100 μg/mL of Liberase™ (Hoffman-La Roche, Switzerland) in PBS to facilitate disassembly into single cells. Mechanical dissociation was performed via pipetting, followed by incubation at 32°C for 40 min. The samples were then centrifuged at 300 r/min for 4 min at 4°C, and the cell pellet was resuspended in 2% fetal bovine serum (FBS) in PBS. The resuspended cells were filtered through a 40 μm nylon mesh filter and washed with 1 mL of PBS, then centrifuged at 300 ×*g* for 4 min and resuspended in 10% FBS and 1% PBS in Dulbecco's Modified Eagle Medium (DMEM) for sequencing.

Sample preparation

Cell suspensions were carefully resuspended in a cold, calcium- and magnesium-free solution containing 0.04% bovine serum albumin (BSA)/PBS. Cell counting was performed using a LUNA-FX7™ Automated Fluorescence Cell Counter (Logos Biosystems, South Korea) with acridine orange (AO) and propidium iodide (PI) staining (Logos Biosystems, South Korea, Cat# F23001). Following this, the cells were processed using a Dead Cells Removal Kit (Miltenyi Biotec, Germany, Cat# 130-090-101) and Magnetic-Activated Cell Sorting (MS) columns (Miltenyi Biotec, Germany, Cat# 130-042-201) in accordance with the manufacturer's guidelines.

Library construction and single-cell RNA sequencing

Single-cell RNA sequencing libraries were prepared using the 10x Chromium Single Cell 5' v2 platform (10x Genomics, USA, document number CG000331), 10x Chromium Controller, and Next Gem Single Cell 5' Reagent v2 kits (10x Genomics, USA, PN-1000244). In brief, the cell suspension, targeting a recovery of 10 000 cells, was combined with a reverse transcription master mix and loaded onto a Single Cell K Chip (10x Genomics, USA, PN-1000286) along with Single Cell 5′ Gel Beads and Partitioning Oil. This process generated Gel Bead-in-Emulsion (GEM) droplets, in which RNA transcripts from single cells were uniquely barcoded and reverse-transcribed. Following GEM formation, barcoded full-length cDNA was synthesized from mRNA during the GEM-RT reaction and subsequently enriched via polymerase chain reaction (PCR). For 5' gene expression library preparation, amplified cDNA underwent enzymatic fragmentation, end-repair, A-tailing, adapter ligation, and index PCR. The purified libraries were quantified using qPCR following the qPCR Quantification Protocol Guide (KAPA) and assessed for quality using the Agilent Technologies 4200 TapeStation (Agilent Technologies, USA). Library sequencing was performed using the HiSeq platform (Illumina, USA).

Single-cell RNA sequencing data processing

The raw sequencing data were processed and demultiplexed using the 10x Genomics Cell Ranger (v.6.0.0) pipeline. Baseline sequencing files were converted into FASTQ file format, after which the sequences were aligned to the *Danio rerio* genome (GRCz11) to generate single-cell feature counts.

All downstream bioinformatic analyses were conducted using the Seurat package (v.4.3.0) (Hao et al., 2021) in R, with default parameters used unless otherwise specified. The analytical approach was consistent with methodologies detailed in our previous studies (Lee et al., 2023a; Lee et al., 2023b; Lee et al., 2024). Quality control measures were implemented to exclude low-quality cells for subsequent analyses. The criteria for exclusion were: (1) Genes expressed in fewer than 12 cells (~0.1% of the data) and cells with fewer than 300 detected genes; (2) Cells expressing more than 3 300 or fewer than 300 unique genes; and (3) Cells with mitochondrial gene content exceeding 10%.

Normalization of raw read counts was performed using the log-normalization method. Highly variable features were identified by applying the "vst" method, selecting the top 2 000 features with the highest variability. To address batch effects and integrate data across samples, the canonical correlation analysis algorithm was used.

Clustering analysis and cell type identification

The integrated single-cell dataset was scaled and processed through principal component analysis (PCA) to reduce dimensionality. The top 22 principal components (PCs) were selected, where the rate of change between consecutive PCs was less than 0.1%. Using the selected PCs, a shared nearest-neighbor graph was constructed, and clustering was performed at a resolution of 0.4. The resulting cell clusters were visualized in two-dimensional (2D) space using Uniform Manifold Approximation and Projection (UMAP).

Cell type annotation was performed by verifying the expression of previously established marker genes using the Zebrafish Information Network (ZFIN, https://zfin.org/) (Bradford et al., 2022), resulting in the identification of 21 cell types: mesenchymal cells (*col6a2*, *col1a2*, and *col1a1b*), keratinocytes (*krt5*, *krtt1c19e*, and *epcam*), epithelial cells (*epcam*), pharynx cells (*cldne* and *dhrs13a.2*), nucleate erythrocytes (RBC) (*hbbe1.1*, *hbbe1.3*, and *hbae3*), fin cells (*and2*, *and1*, and *col1a1a*), radial glia (*fabp7a*, *glula*, *slc1a2b*,

and *atp1a1b*), notochord cells (*col2a1a* and *col9a2*), intestinal epithelial cells (*fabp2* and *epcam*), proliferating cells (*hmgn2*, *hmgb2b*, and *mki67*), myeloid cells (*lcp1*), oligodendrocytes (*mbpa* and *cldnk*), otic vesicle cells (*pax2a* and *stm*), xanthophores (*gch2* and *aox5*), ionocytes (Gill) (*atp1b1b*, *foxi3b*, and *epcam*), olfactory neurons (*pvalb5*, *fstl5*, *s100z*, and *elavl3*), corneal cells (*scinla*), hepatocytes (*apoa1b* and *apoa2*), muscle cells (*ckmb*, *tpma*, *tnnc2*, and *tnnt3b*), and pronephric duct cells (*cdh17* and *dab2*). The expression profiles of these marker genes used for cell type annotation are shown in Supplementary Figure S1.

After identifying the cell types, RBCs were isolated for further sub-cluster analysis. For the sub-clustering process, 22 PCs were used with a resolution of 0.5.

Differentially expressed genes (DEGs) and Gene Ontology (GO) analysis

Clusters constituting more than 5% of the total cell population were analyzed to assess alterations in cell proportions resulting from exposure to polystyrene nanoparticles. Clusters exhibiting the most significant changes were selected for further investigation. DEGs between the control and experimental groups were identified using the Wilcoxon rank-sum test, with criteria of $|\log_2 FC|>0.2$ and adjusted $P<0.05$. GO enrichment analysis was performed on the identified DEGs using ClusterProfiler (v.4.6.2) (Yu et al., 2012) and org.Dr.eg.db (v.3.16.0) (Carlson, 2022), with a cutoff of $P<0.05$ and $Q<0.01$. For analysis of RBC sub-clusters, DEGs were identified using a cutoff of $|\log_2 FC|>0.2$ and $P<0.05$ and subsequent GO analysis was performed with $P<0.05$ and $Q<0.05$.

Calculating gene set module scores

Verification of the GO terms derived from the enrichment analysis was performed by calculating gene set scores using the *AddModuleScore* function (v.2.2.0) (Andreatta & Carmona, 2021) in the Seurat package. Gene sets used for score computation consisted of genes associated with significant GO terms, with details provided in the Supplementary Files.

Inference of cell fate

Cell differentiation trajectories within the RBC cluster were analyzed using the Monocle3 package (v.1.3.1) (Cao et al., 2019). The Seurat object was converted into a Monocle3 cell_data_set object using the *as.cell_data_set* function. Subsequent clustering was performed employing the *cluster_cell* function. The primary graph was constructed in reduced-dimensional space using the *learn_graph* function. The pseudotime starting point was determined based on the expression levels of the *myb* gene, a known marker for hematopoietic stem cells (HSCs) in zebrafish erythropoiesis (Zhang et al., 2021).

***O*-Dianisidine staining**

Sacrificed embryos were stained with a solution containing *o*-dianisidine (0.6 mg/mL), 0.01 mol/L sodium acetate, 0.65% H_2O_2, and 40% (v/v) ethanol for 30 min in a dark environment. The stained embryos were washed in a mixture of ultrapure water and ethanol (6:4, v/v), fixed in 4% paraformaldehyde (PFA) for 1 h, maintained in 3% methylcellulose, and imaged under a microscope.

Reverse transcription-quantitative real-time polymerase chain reaction (RT-qPCR)

Total RNA was extracted from zebrafish embryos using TRIzol reagent (Invitrogen, USA). Chloroform was added to separate protein fractions, and RNA was precipitated using isopropanol. RNA was resuspended in diethyl pyrocarbonate (DEPC)-treated water and reverse-transcribed using SuperScript IV (Thermo Fisher Scientific, USA). RT-qPCR was performed using PowerUp SYBR Green Master Mix (Thermo Fisher Scientific, USA). The expression levels of the target genes were analyzed using the comparative threshold method, and the results were normalized to β- actin as an endogenous control.

Whole-mount *in situ* hybridization

Embryos were fixed in 4% PFA and subsequently dehydrated using methanol. The dehydrated samples were resolved with acetone and incubated at −20°C for one day, followed by thorough washing in acetone. The embryos were incubated in hybridization buffer (500 mL formamide (50%), 250 mL of 20×SSC (5X), 500 μg/mL torula (yeast) RNA, 50 μg/mL heparin, 0.1% 20% Tween-20, 9 mmol/L citric acid, and 225 mL of E-pure water) at 65°C for 2 h, then incubated with anti-DIG *gata1* probe diluted in hybridization buffer at 65°C for 2 days. After incubation, a series of washes were performed at 65°C, including once with hybridization buffer for 1 min, once with 2×SSC for 15 min, and twice with 0.2×SSC for 30 min. The embryos were subsequently incubated in blocking solution (2% heat-inactivated goat serum, 2 mg/mL BSA in PBT [1× PBS+0.1% Tween-20]) for 2 h at room temperature. To detect probe signaling, embryos were incubated overnight at 4°C with a diluted DIG-AP antibody (1:4 000) (Hoffman-La Roche, Switzerland) prepared in the blocking solution. The embryos were then washed with PBT for 15 min. Signal visualization was achieved using 5-bromo-4-chloro-3-indolyl phosphate/nitro blue tetrazolium (BCIP/NBT) dissolved in alkaline phosphatase (AP) buffer, with the samples covered with foil and incubated at room temperature for 4 h. To quench the staining reaction, the embryos were immersed in 1 mmol/L EDTA in 1 mL of 1×PBS and subsequently washed with a solution adjusted to pH 5.2. Excess signals were removed by cleaning the embryos in MeOH for 1 h. Finally, the embryos were imaged using a mounting medium containing 3% methylcellulose.

Fluorescence microscopy of transgenic zebrafish

The erythrocyte-specific marker *gata1*:DsRed was used to identify undifferentiated erythrocytes in transgenic zebrafish. Embryos were anesthetized using a solution of 2 g of tricaine (Sigma-Aldrich, USA) dissolved in 950 mL of E-pure water, with pH adjusted to 7.0 with 1 mol/L Tris. Embryos were imaged under a microscope (SteREO Discovery V8, Zeiss, Germany).

Metabolome extraction

Dechorionated zebrafish embryos, previously freeze-dried and stored at −80°C, were processed for metabolome extraction on the following day. In brief, 1 mL of 0.25% NH_4OH (Fluka, Switzerland) in water, supplemented with 100 ng/mL of an internal standard substance (Coproporphyrin I $^{15}N_4$) (Toronto Research Chemicals, Canada), was added to the prepared sample and vortexed for 1 h. Ultrasonication was subsequently performed for 5 min, followed by the addition of 3 mL of acetonitrile (Tedia, USA) with shaking on a shaker for 5 min. The mixture was then centrifuged at 2 500 ×*g* for 5 min at 4°C to separate the supernatant and protein pellet. The collected supernatant was lyophilized, re-constituted in 1 mL

of 2% formic acid (Sigma-Aldrich, USA) and 80% acetonitrile, and analyzed by liquid chromatography-tandem mass spectrometry (LC-MS/MS) for the quantification of four target analytes. The residual protein pellet was treated with 4 mL of 2% formic acid in 80% acetonitrile supplemented with 100 ng/mL of an internal standard. To enhance protein precipitation, 1 mL of a solution containing 0.1 g of sodium chloride (Merck, Germany) and supersaturated $MgSO_4$ (Junsei Chemical, Japan) was added and shaken on a shaker, followed by centrifugation at 2 500 ×*g* for 5 min at 4°C. A 1 mL aliquot of the organic solution from the upper layer was collected and subjected to LC-MS/TS analysis targeting a specific analyte. Calibration curves for the four analytes were established using diluted solvents consisting of 2% formic acid in 80% acetonitrile. An additional calibration curve was generated for one analyte using a diluted solvent of 2% formic acid in acetonitrile.

LC-MS/MS analysis

Simultaneous quantification of the five analytes was performed using a Shimadzu Nexera X3 LC system and Shimadzu LCMS-8050 triple quadrupole mass spectrometer. Separation was achieved on a Shim-pack GIST C18 Metal Free column (2.1×50 mm, 5 μm). The mobile phase consisted of acetonitrile (solvent A) and a gradient elution system for solvent B with the following program: 0.1% acetonitrile (0.0–0.5 min), 100% acetonitrile (2.7–3.2 min), and 1% acetonitrile (3.3–5.0 min). Electrospray ionization (ESI) was employed as the ionization technique for each target component.

Statistical analysis of data from zebrafish experiments

Statistical analyses of gene expression data were performed using the Student's *t*-test for pairwise comparisons. For experiments involving multiple comparisons, one-way analysis of variance (ANOVA) was used. All experiments were performed in triplicate. A *P*-value less than 0.05 was considered statistically significant.

RESULTS

Characterization of polystyrene nanoparticles

DLS analysis demonstrated that the polystyrene nanoparticles exhibited a uniform size distribution, with an average particle size of 16.7 nm (Figure 1A). The dispersion profiles confirmed the stability and homogeneity of the nanoparticles in the aqueous phase. FTIR spectroscopy further validated the chemical composition of the polystyrene nanoparticles o, revealing characteristic peaks associated with C-H stretching and aromatic rings (Figure 1B) (Hermán et al., 2015). The C-H stretching peaks appeared between 2 800–3 000 cm^{-1}, corresponding to the presence of aliphatic hydrocarbons in the polystyrene structure. Additionally, out-of-plane aromatic C-H vibrations were observed as peaks at approximately 700 cm^{-1}, consistent with the presence of phenyl groups. A distinct O-H stretching vibration peak at approximately 3 400 cm^{-1} suggested surface oxidation or adsorbed water on the nanoparticles . These spectral features collectively confirmed the structural integrity and chemical identity of the polystyrene nanoparticles. HR-TEM analysis of the polystyrene nanoparticles revealed well-defined, spherical nanoparticles with diameters ranging from 10 to 20 nm (average size=14.3 nm) (Figure 1C), consistent with the values obtained from DLS measurements.

Polystyrene nanoparticles impact zebrafish embryo development

Exposure to PS20 nm at a concentration of 10 μg/mL resulted in the highest accumulation within zebrafish embryos (Figure 2A). Despite this, no significant differences in survival rate, overall phenotype, and lateral body length were observed compared to the control (CTRL) group (Figure 2B–D). However, PS20 nm-treated embryos exhibited an increase eye distance in dorsal view (Figure 2E, F) and a significant increase in heart rate (Figure 2G), indicating subtle developmental changes.

Polystyrene nanoparticle exposure alters RBC translation in zebrafish embryos

Quality control analysis of single-cell RNA sequencing data using the Seurat package retained 20 159 cells, including 10 184 from the CTRL group and 9 975 from the PS20 nm-exposed group (Supplementary Figure S1A). Cell-type annotation using established markers identified 20 distinct cell types (Supplementary Figure S1B–D). Subsequent analyses focused on cell types representing over 5% of the total cell population (Supplementary Figure S1E), which included mesenchymal cells (*n*=5 439), keratinocytes (*n*=2 790), epithelial cells (*n*=2 052), pharynx cells (*n*=1 619), RBCs (*n*=1 475), fin cells (*n*=1 389), and notochord cells (*n*=1 061) (Figure 3A) (details regarding the cell types that did not meet these criteria are shown in Supplementary Figure S1). Notable shifts were observed in the pharynx and RBC clusters (Figure 3B; Supplementary Figure S1F, G), with an increased proportion of pharyngeal cells and a decreased proportion of RBCs in the PS20 nm-exposed group.

DEGs in the pharynx cluster were identified between the two groups (Supplementary Table S1). GO analysis of

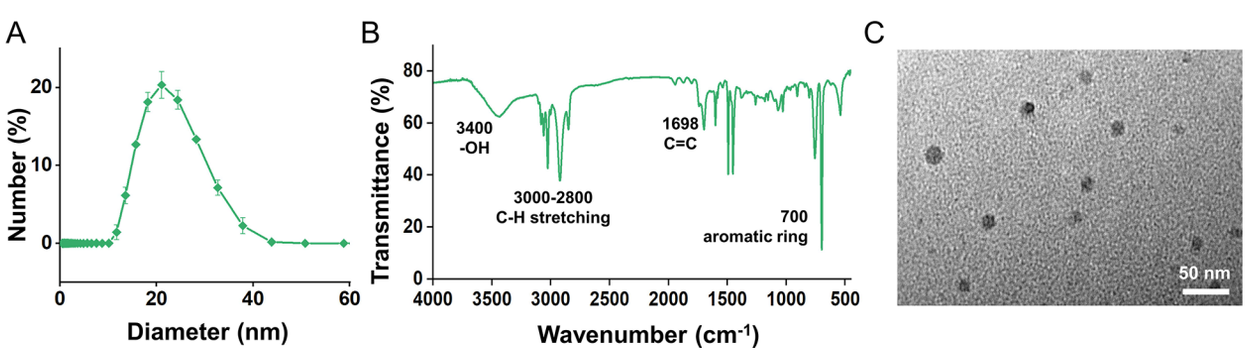

Figure 1 Characterization of polystyrene nanoparticles

A: Dynamic light scattering (DLS) spectra of polystyrene nanoparticles dispersion in water. B: Fourier transform infrared spectroscopy (FTIR) spectra of polystyrene nanoparticles. C: Transmission electron microscopy (TEM) image of polystyrene nanoparticles.

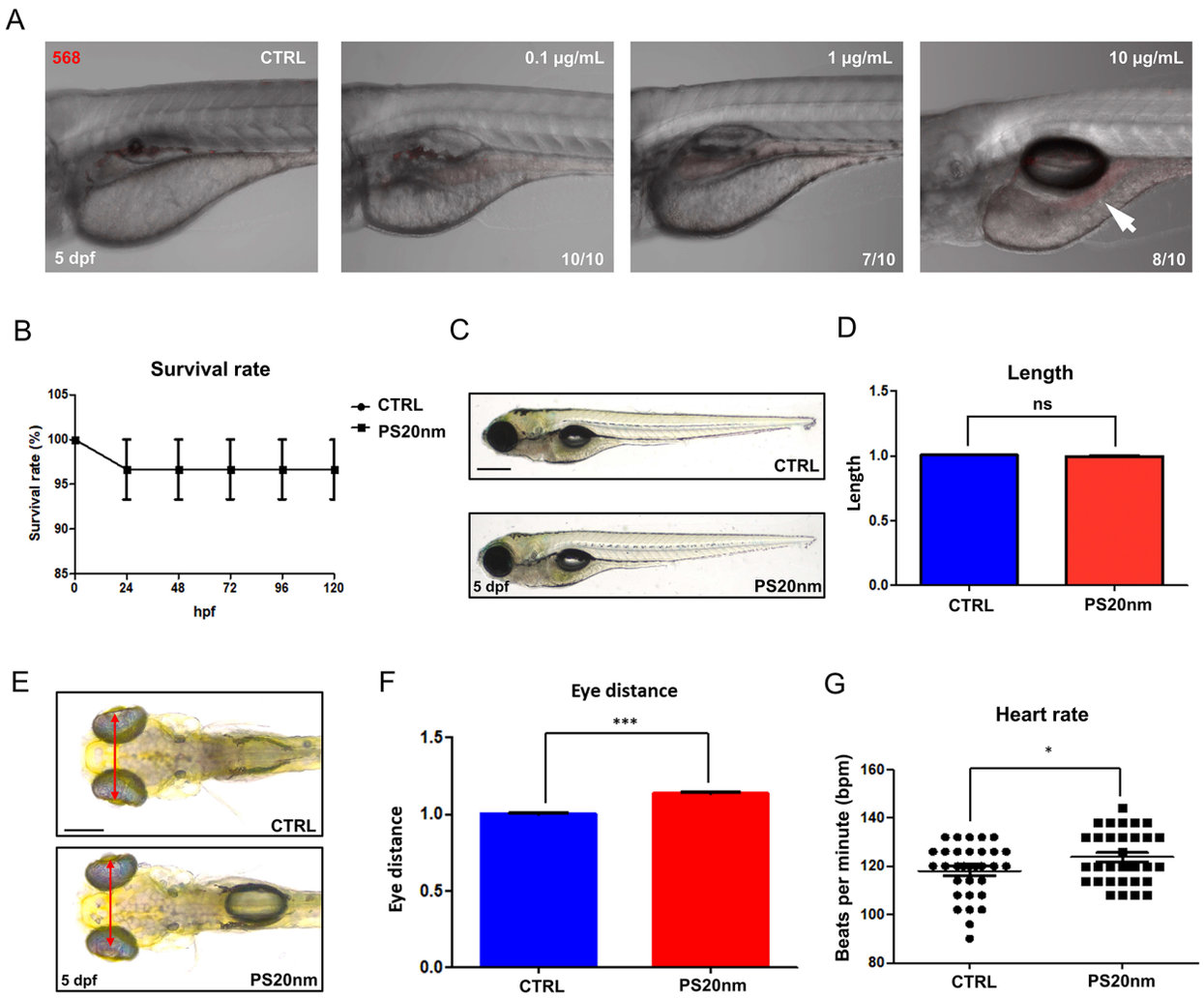

Figure 2 Effects of polystyrene nanoparticles on zebrafish embryo survival and morphology

A: Visualization of polystyrene nanoparticle accumulation in gastrointestinal tract at 0.1 μg/mL, 1 μg/mL, and 10 μg/mL concentrations. B: Effect of polystyrene nanoparticles on survival rate of zebrafish embryos at 5 days post-fertilization (dpf). Values are expressed as mean±SEM (n=30). C: Microscopic observation of zebrafish embryo phenotype following polystyrene nanoparticle treatment. Scale bars: 0.5 mm. D: Quantitative analysis of body length of zebrafish larvae between CTRL and PS20 nm-exposed groups. ns: Not significant. E: Eye distance in 5 dpf zebrafish larvae between CTRL and PS20 nm-exposed groups. Scale bars: 200 μm. F: Quantitative analysis of eye distance in zebrafish larvae, demonstrating a significant increase in the PS20 nm-exposed group compared to the CTRL. ***: P<0.001. G: Measurement of heart rate in zebrafish embryos at 5 dpf after polystyrene nanoparticle exposure. *: P<0.05.

biological processes (GO:BP) revealed an up-regulation of translation-related pathways in the PS20 nm-exposed group (Supplementary Figure S2A and Table S2). To assess the biological relevance of identified GO terms, a list of genes associated with each significant GO term was extracted from the Gene Ontology database (Supplementary Table S3). However, the module scores for the gene set related to translation did not differ significantly between the two groups (Supplementary Figure S2B).

Single-cell RNA sequencing revealed a significant reduction in RBCs upon PS20 nm exposure. This observation was validated using *o*-dianisidine staining, which confirmed a decrease in RBCs in zebrafish embryos following exposure to PS20 nm (Figure 3C). DEG analysis within the RBC cluster identified a global suppression of translation-related pathways and translation-related biological processes in the PS20 nm group (Supplementary Tables S4, S5; Figure 3D). Furthermore, the module scores for both translation and its positive regulation were significantly lower in the PS20 nm-exposed group (Supplementary Figure S2C). Among translation-associated genes, *rps7* demonstrated the most pronounced decrease in expression in the PS20 nm-treated group (Figure 3D, E).

To validate the single-cell RNA sequencing results, *rps7* knockdown experiments were conducted. Knockdown was confirmed by PCR (Figure 3F), and treated embryos exhibited facial malformations and pericardial edema (Figure 3G). In addition, o-dianisidine staining corroborated the reduction in RBCs observed in the PS20 nm-exposed group (Figure 3H).

Polystyrene nanoparticle exposure leads to the formation of immature RBCs

GO:BP analysis of the RBC cluster further revealed significant disruptions in RBC differentiation upon exposure to PS20 nm (Figure 4A; Supplementary Table S5). Based on these observations, we hypothesized that PS20 nm-exposed RBCs would demonstrate distinct differentiation patterns compared to CTRL RBCs. To investigate this, RBC sub-clustering and trajectory analysis were performed (Figure 4B; Supplementary

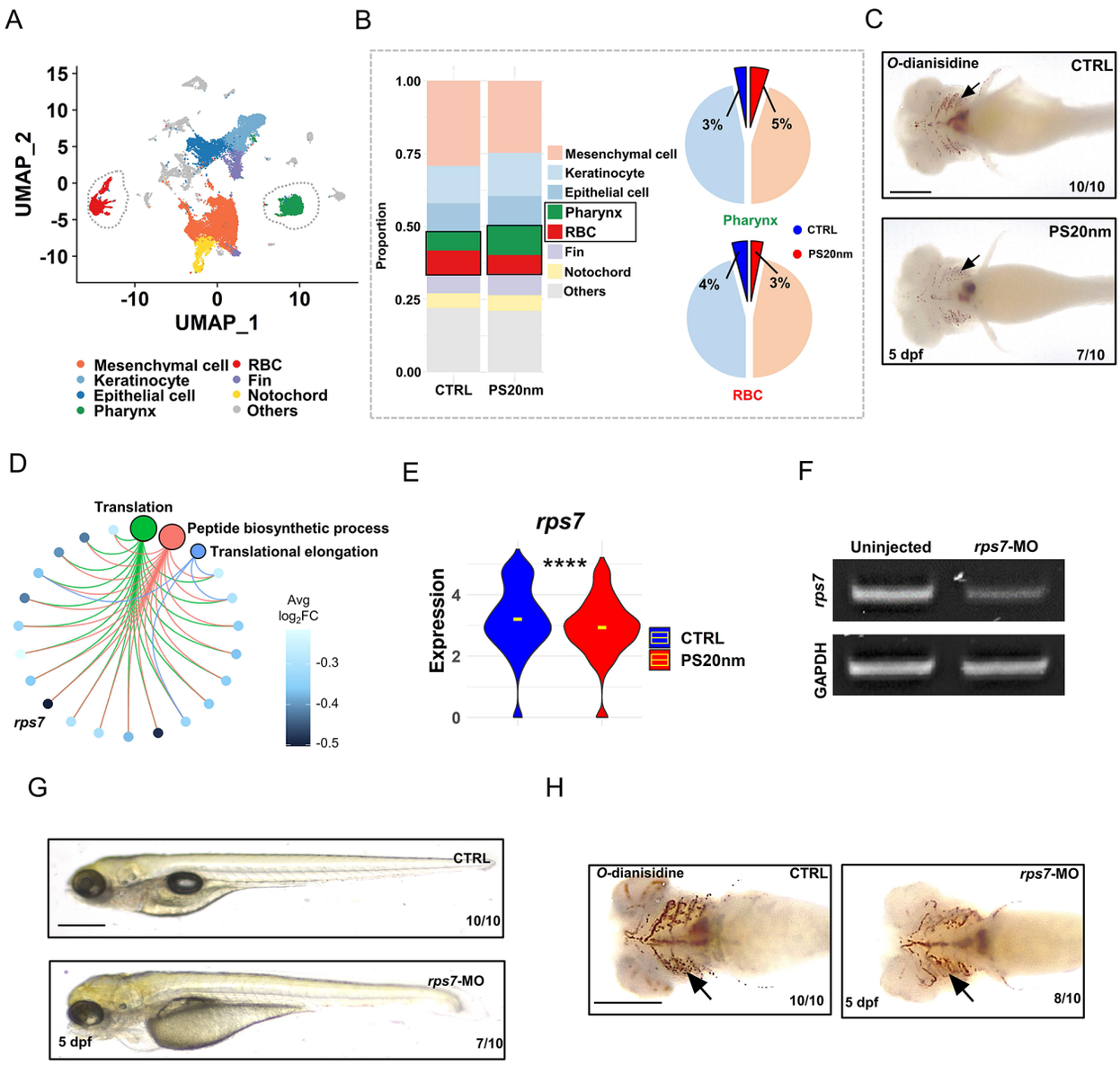

Figure 3 Single-cell RNA sequencing analysis of control and polystyrene nanoparticle-exposed zebrafish

A: UMAP visualization displaying seven cell types accounting for more than 5% of total cell population. B: Bar plots representing the proportion of the seven cell types (left) and pie charts showing notable changes in pharynx cell and RBC proportions between the CTRL and PS20 nm-treated groups (right). C: Examination of embryos from CTRL and PS20 nm-treated groups following o-dianisidine staining. Scale bar: 500 μm. D: Cnetplot showing translation-related terms from GO:BP analysis of RBC cluster. E: Violin plots showing expression levels of *rps7* (****: P<0.0001). F: RT-qPCR analysis of *rps7* and GAPDH in zebrafish embryos at 5 days post-fertilization (dpf). Total RNA was isolated from uninjected embryos and *rps7*-targeting morpholino-injected embryos (3.0 ng). G: Morphological comparison of embryos from uninjected CTRL group and *rps7*-injected group. Scale bars: 0.5 mm. H: Examination of embryos from uninjected CTRL and *rps7*-injected groups following o-dianisidine staining. Scale bar: 500 μm.

Figure S3A). Trajectory inference identified distinct stages of RBC differentiation, with the RBC1 cluster representing early differentiation and the RBC7 cluster representing final differentiation (Supplementary Figure S3A). Differentiation stages within each cluster were annotated using established markers (Figure 4C; Supplementary Figure S3B). Clusters RBC1–4 and 8 exhibited high expression of *myb* and *id1*, indicating HSC-like characteristics (Perry et al., 2007; Singh et al., 2018; Zhang et al., 2021). Clusters RBC5 and 6 were identified as resembling common myeloid progenitors (CMPs) based on the expression of *gata1a* (Zhang et al., 2021). Cluster RBC7, characterized by high expression of *band3* (*slc4a1a*), was determined to represent mature erythrocytes (Martin et al., 2011). A comparison of cell proportions between the CTRL and PS20 nm-exposed groups revealed a substantial increase in CMP-like cells in the PS20 nm-treated group, accompanied by a significant reduction in the proportion of mature erythrocytes (Figure 4D; Supplementary Figure S3C). Further analysis showed elevated expression of *gata1a* in the PS20 nm-exposed group, particularly in the RBC6 cluster, corresponding to CMP-like cells (Figure 4E). These findings suggest that exposure to polystyrene nanoparticles disrupts erythropoiesis in zebrafish, especially during the differentiation of CMP to mature erythrocytes. The expression of *gata1a*, a marker of CMP-like cells, was analyzed to validate the *in silico* findings. Exposure to PS20

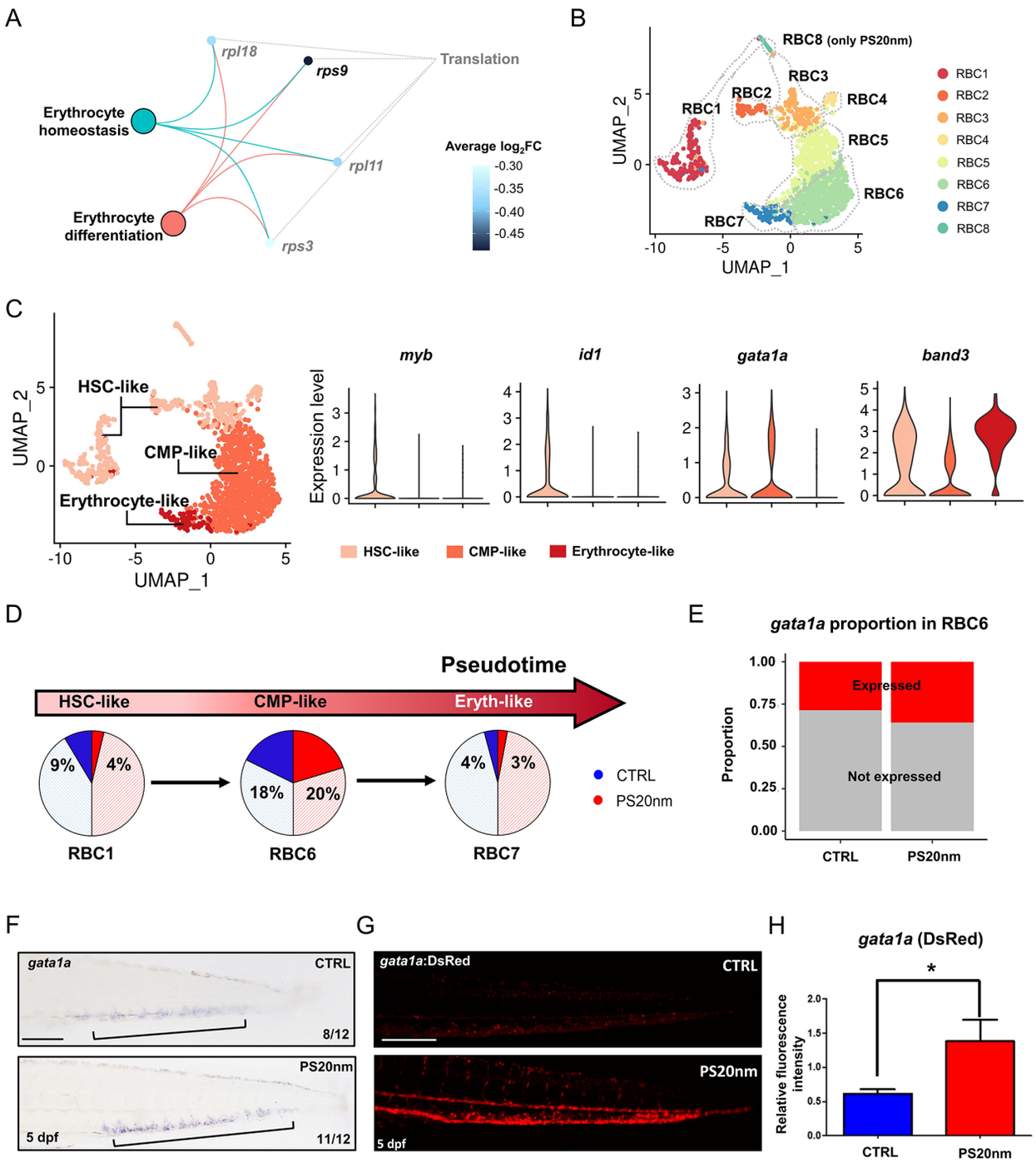

Figure 4 Impaired RBC differentiation in polystyrene nanoparticle-exposed zebrafish embryos identified through RBC sub-cluster analysis

A: Cnetplot illustrating erythropoiesis-related terms from GO:BP analysis of the RBC cluster. B: UMAP representation of RBC sub-clusters. C: Annotation of differentiation stages based on erythropoiesis stage-specific marker genes. D: Pie charts showing changes in cell proportion at each stage of differentiation. E: Bar plot showing proportion of *gata1a*-expressing cells identified in the RBC6 cluster. F: Whole-mount *in situ* hybridization of CTRL and PS20 nm-treated embryos at 5 dpf using erythrocyte marker *gata1a*. Scale bar: 200 μm. G, H: Fluorescence microscopy analysis of *gata1a*-expressing erythrocytes in transgenic zebrafish embryos at 5 dpf and quantification of *gata1a* expression using ImageJ (*: P<0.05). Scale bar: 200 μm.

nm significantly induced the expression of *gata1a* in caudal hematopoietic tissues (CHT), as demonstrated at both the mRNA (Figure 4F) and protein levels (Figure 4G).

Polystyrene nanoparticles impair heme synthesis in mature RBCs

GO:BP analysis of the RBC cluster identified a significant disruption in biological functions associated with heme synthesis following PS20 nm exposure (Figure 5A; Supplementary Table S5). Key genes involved in the heme biosynthesis pathway, including *cpox*, *urod*, and *hsbmb*, were significantly decreased in the PS20 nm-exposed group (Figure 5B; Supplementary Figure S4A). To gain deeper insight into the molecular disruptions, DEG and GO analyses were conducted across all RBC sub-clusters (Supplementary

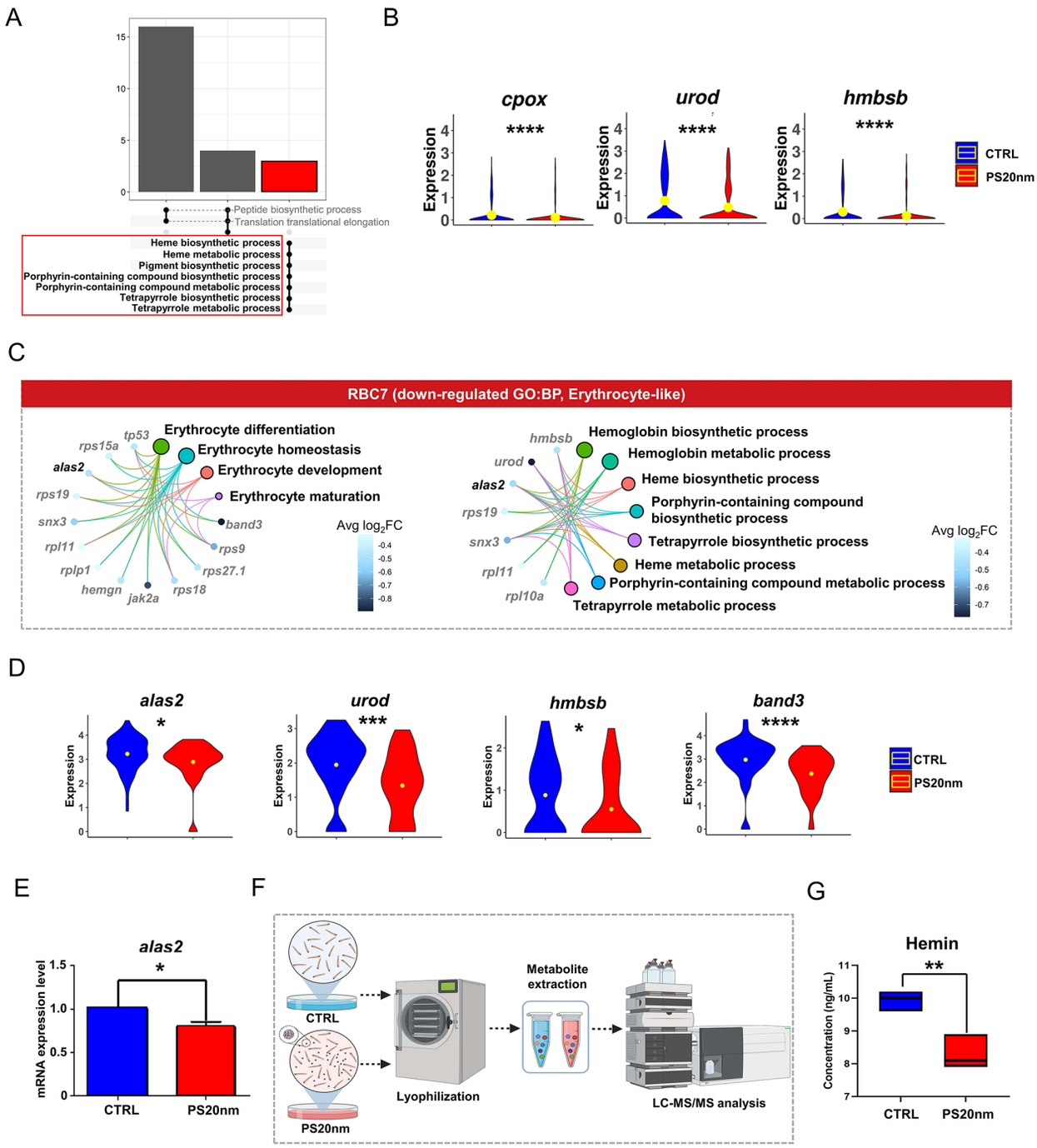

Figure 5 Inhibition of heme synthesis in zebrafish embryos exposed to polystyrene nanoparticles

A: GO:BP analysis highlighting heme synthesis-related terms within the RBC cluster. B: Violin plots showing expression levels of heme synthesis-related genes. ****: $P<0.0001$. C: Representative GO:BP analysis results for RBC7 cluster. D: Violin plots showing expression levels of heme synthesis-related genes in RBC7 cluster, inferred as the final stage of differentiation. E: RT-qPCR analysis of *alas2* expression in PS20 nm-treated embryos compared to untreated CTRL embryos. *: $P<0.05$. F, G: Measurement of hemin concentration in CTRL and PS20 nm-treated embryos using LC-MS/MS (*: $P<0.01$). F was created with BioRender.com.

Table S6). Down-regulation of pathways related to erythrocyte differentiation was observed in the RBC1, RBC6, and RBC7 clusters (Supplementary Figure S4B; Figure 5C). In the RBC1 cluster, *rps* genes associated with erythrocyte differentiation were down-regulated. Similarly, the RBC6 cluster showed down-regulation of genes related to erythrocyte differentiation, including *alas1*, which plays a critical role in the early stages of heme synthesis (Chiabrando et al., 2014). In the RBC7 cluster, pivotal heme synthesis genes, such as *alas2* and *urod*, were significantly down-regulated in the PS20 nm-treated group compared to the CTRL group, highlighting disruptions in erythropoiesis and heme biosynthesis (Chiabrando et al., 2014; Zhang et al., 2021) (Figure 5D).

The expression of *alas2*, a critical gatekeeper gene in heme biosynthesis, was validated in zebrafish embryos using RT-qPCR, confirming a significant reduction in its mRNA levels following PS20 nm exposure (Figure 5E). To further investigate the impact on heme biosynthesis, LC-MS/MS analysis was conducted (Figure 5F), revealing a marked decrease in hemin, the final metabolic product of heme

biosynthetic pathway, in PS20 nm-treated embryos (Figure 5G).

DISCUSSION

Polystyrene, a widely used plastic with a benzene ring structure, is highly reactive and frequently used in nanoplastic research. Nanoparticles with diameters of approximately 20 nm are particularly suitable for toxicity studies due to their ability to cross biological membranes and penetrate cells, enabling accurate assessment of their toxicological effects (Ding et al., 2024). Smaller nanoparticles exhibit a higher surface area-to-volume ratio, enhancing their chemical reactivity, biological interactions, cellular uptake, and tissue penetration (Jin et al., 2019; Shin et al., 2023; Teng et al., 2022). These properties make polystyrene nanoparticles especially valuable for exploring the relationship between toxicity and particle size (Chantho et al., 2024). Additionally, polystyrene is highly prevalent in environmental pollution, underscoring its relevance for toxicity studies. For example, extensive polystyrene microplastic contamination has been detected in river systems such as the Mulde and Elbe, primarily downstream of industrial sources (Laermanns et al., 2021). This environmental prevalence highlights the importance of studying the impact of polystyrene on ecological and biological health.

The concentrations of microplastics and nanoplastics in natural water and marine environments are typically reported to range from 6.35×10^{-3} to 6.94×10^{3} μg/L. However, laboratory studies often employ higher concentrations (1–100 mg/L) to assess the toxicological effects (Wang et al., 2023). In this study, a concentration range of 0.1 to 10 μg/mL was selected, reflecting more environmentally relevant exposure levels. This approach enhances the applicability of our findings and provides insights into potential environmental risks under natural conditions. Notably, zebrafish embryos exposed to a concentration of 10 μg/mL exhibited the highest accumulation of nanoparticles (Figure 2A). Although no severe morphological changes were observed, physiological alterations, including increased eye distance and elevated heart rate, were detected (Figure 2B–G). These findings suggest that polystyrene nanoparticles induce physiological stress responses, even in the absence of overt morphological defects, pointing to potential sub-lethal toxicity.

To assess the biological impacts of polystyrene nanoparticle exposure, zebrafish embryos exposed to 10 μg/mL polystyrene were analyzed using single-cell RNA sequencing (Figure 3A; Supplementary Figure S1). This high-resolution approach enabled precise identification of cellular reactions and gene expression alterations induced by nanoparticle exposure (Figure 3). While prior research has reported gut cell damage after prolonged exposure to 500 ng/mL polystyrene nanoparticles for 28 days (Deng et al., 2023), our study demonstrated significant effects on pharynx cells and RBCs within just 48 h of exposure (Figure 3B). Specifically, genes involved in translation in the RBC cluster showed marked down-regulation, correlating with reduced expression of genes crucial for erythropoiesis, such as *rps7* (Figure 3D–H). These results align with recent research demonstrating a reduction in erythrocyte production in zebrafish after treatment with silver nanoparticles (Cui et al., 2016). The single-cell RNA sequencing data indicated a widespread reduction in the expression of genes associated with translation (Supplementary Figure S2C), suggesting a pathological mechanism similar to that of Diamond-Blackfan anemia (DBA), a disorder associated with insufficient expression of ribosome-related genes, such as *rps19*, *rps24*, and *rps17* (Chen et al., 2020; Doherty et al., 2010). Interestingly, in PS20 nm-exposed zebrafish embryos, neither *p53* nor *TNF-α* expression was elevated (data not shown), which are hallmark mechanisms of DBA. However, facial deformities (Figure 2E, F) and a significant reduction in erythrocyte number (Figure 3B, C) were observed. These disruptions to erythropoiesis could lead to anemia-like symptoms, resulting in reduced physical performance, impaired feeding activity, and potential organ damage (Chiabrando et al., 2014).

Hematopoiesis in zebrafish embryos occurs in three distinct waves: primitive, transient, and definitive (Davidson & Zon, 2004). The primitive wave initiates the generation of blood cells to supply oxygen and establish the immune system (Davidson & Zon, 2004; Kulkeaw & Sugiyama, 2012). The transient wave serves as an intermediate stage, producing some blood cells and leading to the emergence of temporary blood components (Zhang et al., 2021). The definitive wave drives the formation of all blood cell types, establishing the complete hematopoietic system (Hu & Jing, 2023). This study focused on the hematopoietic process during the transient wave to investigate erythrocyte differentiation under polystyrene nanoparticle exposure. Representative gene expression levels, including *cmyb* (*myb*) and *gata1a*, were analyzed to track the erythropoietic process (Figure 4C). Results revealed that erythrocyte differentiation was arrested at the CMP stage (Figure 4D–H), resulting in the accumulation of immature erythrocytes and disrupted erythrocyte differentiation. Previous studies have examined the long-term effects of micro- and nanoplastics on hematopoiesis. For example, (Jing et al., 2022) investigated mammalian models exposed to micro-/nanoplastics for 42 days, identifying erythrocyte reductions linked to changes in HSCs mediated by interactions with gut microbiota and cytokines. In contrast, our zebrafish embryonic model with a shorter exposure duration (48 h) did not show alterations in HSCs within the CHT (Supplementary Figure S5A). Instead, polystyrene nanoparticles directly impacted translation-related pathways and RBC differentiation. These findings provide insights into how polystyrene nanoparticles disrupt erythrocyte differentiation, leading to a reduction in erythrocytes, and emphasize the importance of examining the effects of nanoplastic exposure on erythrocyte differentiation under varied conditions.

Single-cell RNA sequencing indicated a general decline in the expression of genes associated with translation and heme synthesis (Figure 5A). GO analysis further highlighted a marked decrease in the expression of key genes involved in heme synthesis, including *cpox*, *urod*, and *hmbsb*, implying a reduction in the availability of heme metabolites required for erythropoiesis (Figure 5B). Notably, the expression of *alas2*, a critical regulator in the heme biosynthesis pathway, was significantly reduced at the mRNA level (Figure 5D, E). Due to the low abundance of heme in zebrafish embryos and the limitations of traditional quantification methods, LC-MS/MS was employed to measure heme metabolites (Figure 5F), a technique previously used to quantify linezolid and heme concentrations in infected individuals and their relationship (Feng et al., 2022). In this study, LC-MS/MS analysis confirmed a notable reduction in heme metabolites in zebrafish embryos following the administration of polystyrene

nanoparticles (Figure 5G). These findings provide compelling evidence that polystyrene nanoparticles inhibit heme biosynthesis, leading to impaired erythropoiesis.

Extensive research has investigated the toxic effects of polystyrene nanoparticles on aquatic organisms, primarily focusing on oxidative stress and inflammation (Feng et al., 2022; Pei et al., 2022; Wu et al., 2022). However, the impact of polystyrene nanoparticles on erythropoiesis remains poorly understood. This study validated results from single-cell RNA sequencing through *in vivo* analysis, confirming disruptions at the mRNA level. Despite these insights, additional validation via proteomic approaches and comprehensive investigation into the entire hematopoietic process are necessary to fully elucidate the toxicological mechanisms. Nonetheless, this study revealed that exposure to polystyrene nanoparticles inhibits translation and heme synthesis, leading to the formation of immature erythrocytes. These findings highlight the toxic effects of polystyrene nanoparticles on erythropoiesis and underscore the importance of investigating diverse biological responses to nanoparticle exposure, which should contribute to a broader understanding of hematological impacts on aquatic organisms.

The observed reduction in RBCs and development of anemia resulting from exposure to polystyrene nanoparticles can pose significant risks to both animal populations and ecosystems. Reduced RBC levels impair oxygen transport, leading to diminished physical capabilities, impaired feeding behaviors, increased organ damage, and compromised immune systems (Canny et al., 2023; Ekiz et al., 2005). These physiological impairments may cascade into reduced reproduction and survival rates, disrupting population dynamics and ecosystem balance. As a result, the hematological disruptions induced by polystyrene nanoparticles may have far-reaching consequences that extend beyond individual organisms, impacting the ecosystem as a whole.

This study is the first to specifically investigate the effects of nanoparticles on RBCs, serving as a foundational pilot study for future research on how various nanoparticles influence erythropoiesis. Our findings demonstrated that exposure to polystyrene nanoparticles at a concentration of 10 μg/mL significantly disrupted erythropoiesis in zebrafish embryos. By interfering with translation and heme synthesis pathways, these nanoparticles caused an accumulation of immature erythrocytes. Importantly, the selected concentration reflects realistic environmental levels, accounting for regional and ecological variability. The significant disruption of erythropoiesis observed in this study underscores the potential risks posed by nanoparticle pollution in aquatic ecosystems. These findings highlight the urgent need for further research to explore the full extent of environmental and biological impacts of polystyrene nanoparticles, particularly regarding their implications for organismal health and ecosystem stability.

DATA AVAILABILITY

All single-cell RNA sequencing data used for this study are available at Gene Expression Omnibus (GEO, https://www.ncbi.nlm.nih.gov/geo/) under accession number GSE270075.

SUPPLEMENTARY DATA

Supplementary data to this article can be found online.

COMPETING INTERESTS

The authors declare that they have no competing interests.

AUTHORS' CONTRIBUTIONS

Conceptualization: C.-K.O. and Y.H.K.; Characterization of polystyrene nanoparticles: S.J.; *In silico* experiments: E.J.K. and H.L.; *In vivo* experiments: H.M.S., S.A., Y.K., and C.R.L.; Funding acquisition: E.J.K., K.M., C.-K.O., and Y.H.K.; Writing the manuscript: E.J.K. and H.M.S.; Reviewing the manuscript: K.M., K.K., W.K.K., and D.K., Supervising the research: C.-K.O., S.J., and Y.H.K. All authors read and approved the final version of the manuscript.

ACKNOWLEDGMENTS

We would like to thank Nuri Lim and Youngmin Hong from the Shimadzu Corporation for their assistance with LC-MS/MS analysis of heme metabolites. The authors thank all members of DecodeCell Inc. and Macrogen Inc. for helpful comments and discussions.

REFERENCES

Alimi OS, Claveau-Mallet D, Kurusu RS, et al. 2022. Weathering pathways and protocols for environmentally relevant microplastics and nanoplastics: what are we missing?. *Journal of Hazardous Materials*, **423**: 126955.

Andrady AL. 2011. Microplastics in the marine environment. *Marine Pollution Bulletin*, **62**(8): 1596–1605.

Andrady AL, Neal MA. 2009. Applications and societal benefits of plastics. *Philosophical Transactions of the Royal Society B Biological Sciences*, **364**(1526): 1977–1984.

Andreatta M, Carmona SJ. 2021. UCell: Robust and scalable single-cell gene signature scoring. *Computational and Structural Biotechnology Journal*, **19**: 3796–3798.

Bradford YM, Van Slyke CE, Ruzicka L, et al. 2022. Zebrafish information network, the knowledgebase for *Danio rerio* research. *Genetics*, **220**(4): iyac016.

Canny SP, Orozco SL, Thulin NK, et al. 2023. Immune mechanisms in inflammatory anemia. *Annual Review of Immunology*, **41**: 405–429.

Cao JY, Spielmann M, Qiu XJ, et al. 2019. The single-cell transcriptional landscape of mammalian organogenesis. *Nature*, **566**(7745): 496–502.

Carlson M. 2022. org. Dr. eg. db: Genome wide annotation for Zebrafish. https://bioconductor.org/packages/release/data/annotation/html/org.Dr.eg.db.html.

Chantho V, Sillapaprayoon S, Saenmuangchin R, et al. 2024. Effects of polystyrene nanoplastic size on zebrafish embryo development. *Toxicology in Vitro*, **99**: 105868.

Chen C, Lu MJ, Lin S, et al. 2020. The nuclear gene *rpl18* regulates erythroid maturation via JAK2-STAT3 signaling in zebrafish model of diamond-blackfan anemia. *Cell Death & Disease*, **11**(2): 135.

Cheng HD, Duan ZH, Wu YH, et al. 2022. Immunotoxicity responses to polystyrene nanoplastics and their related mechanisms in the liver of zebrafish (*Danio rerio*) larvae. *Environment International*, **161**: 107128.

Chiabrando D, Mercurio S, Tolosano E. 2014. Heme and erythropoieis: more than a structural role. *Haematologica*, **99**(6): 973–983.

Cole M, Lindeque P, Fileman E, et al. 2013. Microplastic ingestion by zooplankton. *Environmental Science & Technology*, **47**(12): 6646–6655.

Cui B, Ren L, Xu QH, et al. 2016. Silver_ nanoparticles inhibited erythrogenesis during zebrafish embryogenesis. *Aquatic Toxicology*, **177**: 295–305.

Davidson AJ, Zon LI. 2004. The 'definitive' (and 'primitive') guide to zebrafish hematopoiesis. *Oncogene*, **23**(43): 7233–7246.

Deng JW, Zeng XL, Li JJ, et al. 2023. Single-cell transcriptomic analysis reveals heterogeneity of the patterns of responsive genes and cell communications in liver cell populations of zebrafish exposed to polystyrene nanoplastics. *Science of the Total Environment*, **889**: 164082.

Ding RY, Chen YY, Shi XM, et al. 2024. Size-dependent toxicity of polystyrene microplastics on the gastrointestinal tract: Oxidative stress

related-DNA damage and potential carcinogenicity. *Science of the Total Environment*, **912**: 169514.

Doherty L, Sheen MR, Vlachos A, et al. 2010. Ribosomal protein genes RPS10 and RPS26 are commonly mutated in diamond-blackfan anemia. *The American Journal of Human Genetics*, **86**(2): 222–228.

Duis K, Coors A. 2016. Microplastics in the aquatic and terrestrial environment: sources (with a specific focus on personal care products), fate and effects. *Environmental Sciences Europe*, **28**(1): 2.

Ekiz C, Agaoglu L, Karakas Z, et al. 2005. The effect of iron deficiency anemia on the function of the immune system. *The Hematology Journal*, **5**(7): 579–583.

Ekvall MT, Lundqvist M, Kelpsiene E, et al. 2019. Nanoplastics formed during the mechanical breakdown of daily-use polystyrene products. *Nanoscale Advances*, **1**(3): 1055–1061.

Feng ML, Luo JJ, Wan YP, et al. 2022. Polystyrene nanoplastic exposure induces developmental toxicity by activating the oxidative stress response and base excision repair pathway in zebrafish (*Danio rerio*). *ACS Omega*, **7**(36): 32153–32163.

Gu WQ, Liu S, Chen L, et al. 2020. Single-cell RNA sequencing reveals size-dependent effects of polystyrene microplastics on immune and secretory cell populations from zebrafish intestines. *Environmental Science & Technology*, **54**(6): 3417–3427.

Hao YH, Hao S, Andersen-Nissen E, et al. 2021. Integrated analysis of multimodal single-cell data. *Cell*, **184**(13): 3573–3587. e29.

Hermán V, Takacs H, Duclairoir F, et al. 2015. Core double–shell cobalt/graphene/polystyrene magnetic nanocomposites synthesized by *in situ* sonochemical polymerization. *RSC Advances*, **5**(63): 51371–51381.

Hu YX, Jing Q. 2023. Zebrafish: a convenient tool for myelopoiesis research. *Cell Regeneration*, **12**(1): 2.

Jambeck JR, Geyer R, Wilcox C, et al. 2015. Plastic waste inputs from land into the ocean. *Science*, **347**(6223): 768–771.

Jiang WL, Liu YL, Wu YQ, et al. 2024. Polystyrene nanoplastics of different particle sizes regulate the polarization of pro-inflammatory macrophages. *Scientific Reports*, **14**(1): 16329.

Jin YX, Lu L, Tu WQ, et al. 2019. Impacts of polystyrene microplastic on the gut barrier, microbiota and metabolism of mice. *Science of the Total Environment*, **649**: 308–317.

Jing JR, Zhang L, Han L, et al. 2022. Polystyrene micro-/nanoplastics induced hematopoietic damages via the crosstalk of gut microbiota, metabolites, and cytokines. *Environment International*, **161**: 107131.

Kik K, Bukowska B, Sicińska P. 2020. Polystyrene nanoparticles: sources, occurrence in the environment, distribution in tissues, accumulation and toxicity to various organisms. *Environmental Pollution*, **262**: 114297.

Kulkeaw K, Sugiyama D. 2012. Zebrafish erythropoiesis and the utility of fish as models of anemia. *Stem Cell Research & Therapy*, **3**(6): 55.

Laermanns H, Reifferscheid G, Kruse J, et al. 2021. Microplastic in water and sediments at the confluence of the elbe and mulde rivers in Germany. *Frontiers in Environmental Science*, **9**: 794895.

Law KL, Thompson RC. 2014. Microplastics in the seas. *Science*, **345**(6193): 144–145.

Lee H, Joo JY, Kang J, et al. 2023a. Single-cell analysis of platelets from patients with periodontitis and diabetes. *Research and Practice in Thrombosis and Haemostasis*, **7**(2): 100099.

Lee H, Joo JY, Song JM, et al. 2023b. Immunological link between periodontitis and type 2 diabetes deciphered by single-cell RNA analysis. *Clinical and Translational Medicine*, **13**(12): e1503.

Lee H, Park S, Yun JH, et al. 2024. Deciphering head and neck cancer microenvironment: single-cell and spatial transcriptomics reveals human papillomavirus-associated differences. *Journal of Medical Virology*, **96**(1): e29386.

Martin CS, Moriyama A, Zon LI. 2011. Hematopoietic stem cells, hematopoiesis and disease: lessons from the zebrafish model. *Genome Medicine*, **3**(12): 83.

Ogonowski M, Schür C, Jarsén Å, et al. 2016. The effects of natural and anthropogenic microparticles on individual fitness in daphnia magna. *PLoS One*, **11**(5): e0155063.

Pedersen AF, Meyer DN, Petriv AMV, et al. 2020. Nanoplastics impact the zebrafish (*Danio rerio*) transcriptome: associated developmental and neurobehavioral consequences. *Environmental Pollution*, **266**: 115090.

Pei X, Heng X, Chu WH. 2022. Polystyrene nano/microplastics induce microbiota dysbiosis, oxidative damage, and innate immune disruption in zebrafish. *Microbial Pathogenesis*, **163**: 105387.

Perry SS, Zhao Y, Nie L, et al. 2007. Id1, but not Id3, directs long-term repopulating hematopoietic stem-cell maintenance. *Blood*, **110**(7): 2351–2360.

Ryan PG, Moore CJ, Van Franeker JA, et al. 2009. Monitoring the abundance of plastic debris in the marine environment. *Philosophical Transactions of the Royal Society B Biological Sciences*, **364**(1526): 1999–2012.

Schwarz AE, Ligthart TN, Boukris E, et al. 2019. Sources, transport, and accumulation of different types of plastic litter in aquatic environments: a review study. *Marine Pollution Bulletin*, **143**: 92–100.

Shen M C, Zhang Y X, Zhu Y, et al. 2019. Recent advances in toxicological research of nanoplastics in the environment: a review. *Environmental Pollution*, **252**: 511–521.

Shin HS, Lee SH, Moon HJ, et al. 2023. Exposure to polystyrene particles causes anxiety-, depression-like behavior and abnormal social behavior in mice. *Journal of Hazardous Materials*, **454**: 131465.

Singh SK, Singh S, Gadomski S, et al. 2018. Id1 ablation protects hematopoietic stem cells from stress-induced exhaustion and aging. *Cell Stem Cell*, **23**(2): 252–265. e8.

Sökmen TÖ, Sulukan E, Türkoğlu M, et al. 2020. Polystyrene nanoplastics (20 nm) are able to bioaccumulate and cause oxidative DNA damages in the brain tissue of zebrafish embryo (Danio rerio). *Neurotoxicology*, **77**: 51–59.

Teng MM, Zhao XL, Wang CJ, et al. 2022. Polystyrene nanoplastics toxicity to zebrafish: dysregulation of the brain-intestine-microbiota axis. *ACS Nano*, **16**(5): 8190–8204.

Thushari GGN, Senevirathna JDM. 2020. Plastic pollution in the marine environment. *Heliyon*, **6**(8): e04709.

Timilsina A, Adhikari K, Yadav AK, et al. 2023. Effects of microplastics and nanoplastics in shrimp: Mechanisms of plastic particle and contaminant distribution and subsequent effects after uptake. *Science of the Total Environment*, **894**: 164999.

Wang T, Li BJ, Zou XQ, et al. 2019. Emission of primary microplastics in mainland China: invisible but not negligible. *Water Research*, **162**: 214–224.

Wang WY, Mao X, Zhang R, et al. 2023. Nanoplastic exposure at environmental concentrations disrupts hepatic lipid metabolism through oxidative stress induction and endoplasmic reticulum homeostasis perturbation. *Environmental Science & Technology*, **57**(38): 14127–14137.

Wu H, Guo JM, Yao YJ, et al. 2022. Polystyrene nanoplastics induced cardiomyocyte apoptosis and myocardial inflammation in carp by promoting ROS production. *Fish & Shellfish Immunology*, **125**: 1–8.

Yu GC, Wang LG, Han YY, et al. 2012. clusterProfiler: an R package for comparing biological themes among gene clusters. *OMICS: A Journal of Integrative Biology*, **16**(5): 284–287.

Zhang YH, Chen MY, Chen CY. 2021. Using the zebrafish as a genetic model to study erythropoiesis. *International Journal of Molecular Sciences*, **22**(19): 10475.

Zhu XY, Peng L, Song EQ, et al. 2022. Polystyrene nanoplastics induce neutrophil extracellular traps in mice neutrophils. *Chemical Research in Toxicology*, **35**(3): 378–382.